

Article

Dynamic Characteristics Study of Elastic Ring Squeeze Film Damper with Rigid–Elastic–Oil Coupled Model

Yan Li, Haisheng Yang and Sier Deng *

School of Mechatronics Engineering, Henan University of Science and Technology, Luoyang 471003, China; lytangshao@163.com (Y.L.); yhs1975@163.com (H.Y.)

* Correspondence: dse@haust.edu.cn

Abstract: Due to the coupling of the damper journal with the elastic ring and oil film, the elastic ring squeeze film damper (ERSFD) shows better dynamic performance in comparison with the traditional squeeze film damper (SFD). Therefore, a novel rigid–elastic–oil coupled mathematical model was established. The elastic ring deformation, as the key point, is solved according to the planar bending theory. Then, based on the pressure governing equation of the oil film, using the central finite difference method, the oil film pressure was addressed. Meanwhile, the Simpson method was implemented to calculate the dynamic characteristic coefficients (equivalent stiffness and damping C_e) of ERSFD (DCCEs). Also, we analyzed the influence of journal eccentricity, oil film radius clearance, flexibility coefficient and damping hole diameter on the DCCEs, and the results were compared and verified with the existing literature. The sensitivity of each parameter to the DCCEs was analyzed by using the linear regression method. According to the results, the flexibility coefficient has the greatest effect on the DCCEs, followed by the oil film radius clearance. The eccentricity of the journal and damping hole diameter have the least impact. This work will provide a theoretical basis for reflecting on the bearing dynamic characteristics more truly and accurately.

Keywords: ERSFD; rigid–elastic–oil coupled model; planar bending theory; DCCEs; flexibility coefficient; sensitivity



Citation: Li, Y.; Yang, H.; Deng, S. Dynamic Characteristics Study of Elastic Ring Squeeze Film Damper with Rigid–Elastic–Oil Coupled Model. *Lubricants* **2023**, *11*, 491. <https://doi.org/10.3390/lubricants11110491>

Received: 10 October 2023
Revised: 4 November 2023
Accepted: 10 November 2023
Published: 12 November 2023



Copyright: © 2023 by the authors. Licensee MDPI, Basel, Switzerland. This article is an open access article distributed under the terms and conditions of the Creative Commons Attribution (CC BY) license (<https://creativecommons.org/licenses/by/4.0/>).

1. Introduction

In order to effectively suppress vibrations in a nonlinear rotor-bearing system, the main bearing is usually equipped with a squeeze film damper [1–4]. In addition to the improvement in the stable operating speed margin, the critical speed of the rotor system is efficiently adjusted using the ERSFD. Apparently, oil film damping greatly attenuates the vibration response of the rotor system, under the condition that it passes via the critical speed, and also lowers the external excitation force [5]. However, the high nonlinearity of the oil film stiffness makes it difficult for the rotor system to pass the critical speed, which may also cause uncoordinated responses such as bistable jump [6–9]. Under nonworking conditions, the journal surface of the damper can also be separated from the bearing surface, and the journal does not contact the bearing surface by appropriate anti-gravity preloading of this structure. The squeeze oil film damper produces nonlinear oil film force on the main bearing, which makes the outer ring perform free precession in the plane, changes the load distribution inside the bearing, and thus affects the dynamic characteristics of each component of the bearing. Therefore, it is necessary to further study the dynamic characteristics of ERSFD and determine the oil film force sensitive factors so as to analyze the dynamic characteristics of bearings more truly and accurately.

The structure of spindle bearing and elastic support tends to be integrated [10–12], forming a rigid–elastic–oil coupled ERSFD structure. As shown in Figure 1, an elastic ring is arranged between the journal (the bearing outer ring) and the bearing pedestal, which classifies the oil film cavity into both the inner and outer layers. On both the inner and outer

sides of the elastic ring, numerous bosses are evenly distributed. Clearly, the outer diameter of the damper journal together with the inner diameter of the elastic ring can form the inner oil film chamber of the ERSFD, whereas we can also constitute the outer oil film chamber of the ERSFD by the inner diameter of the bearing pedestal and the outer diameter of the elastic ring. Apart from that, the elastic ring can restrict its rotation relative to the bearing pedestal through the brake pin. Meanwhile, through the damping holes on the elastic ring, we can connect the inner and outer oil film cavities. Regarding the rigid–elastic–oil coupled ERSFD structure, the journal squeezes the oil film under the action of unbalanced force when the rotor works at high speed, and the inner bosses of the elastic ring bear the contact force of the journal. It is found that the elastic ring deformation generates the increasing oil film thickness in the inner cavity, which can inhibit the dramatical elevation of the radial oil film force. In addition, with the rotor working at low speed, due to the weakening of the oil film squeeze and shear, the elastic ring deformation recovers and the oil film clearance in the inner cavity decreases, thus limiting the excessive decrease in the oil film force. Additionally, vibration energy can be generated with the journal contacting the elastic ring and squeezing the oil film on the basis of the influence. Simultaneously, part of the vibration energy can be absorbed by the oil film damping. In addition, the elastic ring stores excess energy and slowly releases it within the deformation. Through the outer bosses, the exciting force is transmitted to the bearing pedestal and finally to the casing.

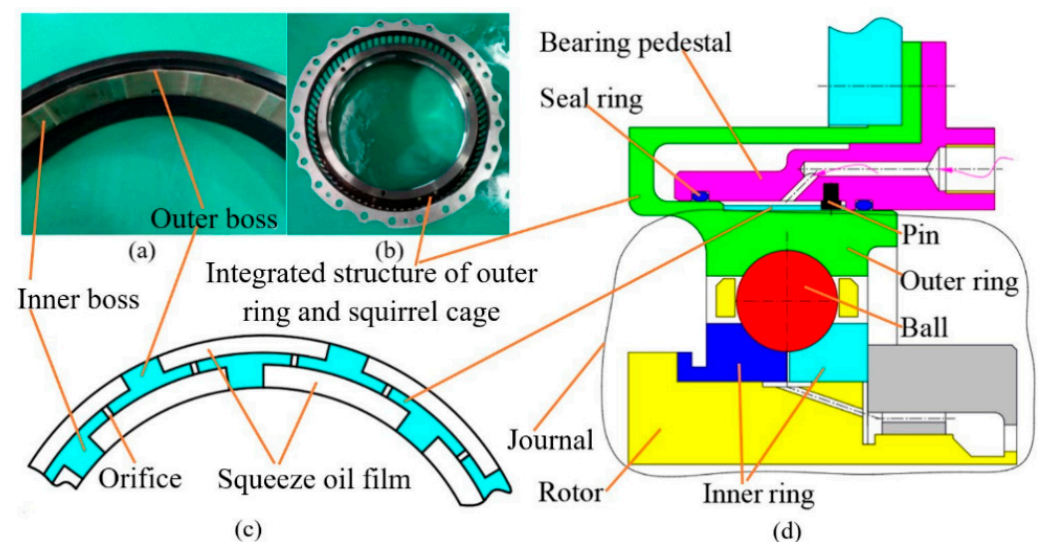


Figure 1. Diagram of rigid–elastic–oil coupled structure. (a) The elastic ring location in ERSFD. (b) Integrated structure of outer ring and squirrel cage. (c) Partial structure diagram of the elastic ring. (d) ERSFD.

In recent years, many scholars have carried out extensive studies on the dynamic characteristics of ERSFD. Zhou [13] obtained the governing equations of the inner and outer oil film of ERSFD in accordance with the generalized Reynolds equation and compared as well as analyzed the characteristics of the Reynolds equation of ERSFD and SFD, also pointing out that ERSFD combined the advantages of elastic support and SFD. This is because the oil film damping is increased by the segmented oil film and the complex fluid–solid interaction. Moreover, the highly nonlinear oil film stiffness caused by the elevation of the unbalanced force is improved. According to the finite element method, Hong et al. [14] analyzed the reason why ERSFD effectively inhibited nonlinear vibrations. When the eccentricity increases, the oil film pressure and the elastic ring deformation are coupled to offset part of the increment of eccentricity and also weaken the nonlinear increase trend in the oil film force. Xu et al. [15] used Finite element method (FEM) to explore the impact of the oil permeation holes distribution on the oil film damping features of ERSFD. On the basis of the obtained results, the distribution of the oil permeation holes can adjust the damping coefficient. Based on the methods of experimental and numerical

analysis, Li et al. [16] explored the influence rules of factors, such as the boss height of the elastic ring, the oil supply conditions, and the unbalance, on the dynamic characteristics of ERSFD. The findings show that when the height of the elastic ring boss is small and equivalent to 0.5 mm, the nonlinearity of the oil film can be effectively improved. Based on the Kirchhoff hypothesis, Han et al. [17] established a finite element model of an elastic ring based on shell elements, determined the relationship between elastic ring deformation, oil film force and rotor motion, and analyzed the oil film coefficient of ERSFD and the dynamic response of the rotor system. The analysis indicates that the nonlinearity of the ERSFD oil film coefficient is lower than that of SFD. Shi et al. [18] established the rotor dynamic model with a novel floating ring squeeze oil film damper (FSFD) and identified the oil film pressure distribution, fluid–structure coupling dynamic characteristics and elastic ring support stiffness of the rotor system with FSFD. The results show that the small-scale and low stiffness FSFD has a significant regulating effect on rotor vibration. Zhao et al. [19] explored the dynamic characteristics of ERSFD by considering the influence of damping holes and obtained the variation of equivalent stiffness and damping with eccentricity. Even though the abovementioned literature elaborates on the highly nonlinear mechanism of ERSFD increasing the oil film damping and improving the oil film stiffness, it does not study the influence rule of relevant parameters on the DCCEs.

For the DCCEs, some scholars have carried out a deeper study. Cao et al. [20] studied the oil film force characteristics of ERSFD through solving the mathematical and physical model of ERSFD and compared and explored the changing rules of oil film stiffness and damping based on different boundary conditions. As shown by the obtained findings, the equivalent stiffness and damping of ERSFD are not affected by the presence or absence of oil seepage holes. With end sealing, the equivalent stiffness and damping are significantly higher than those without end sealing. The ERSFD with end sealing and oil permeating holes shows better linear stiffness characteristics, but the eccentricity has little influence on the equivalent damping. Based on the finite element analysis and the squeeze oil film theory, He Hong et al. [21] analyzed and studied the oil film stiffness and damping. The results show that ERSFD can effectively improve the coupling problem of degrees of freedom regarding oil film stiffness and damping and finally significantly suppress the nonlinearity of oil film stiffness and damping, which vary with the eccentricity. Wang et al. [22] established the finite element model of the elastic ring on the basis of the thick plate element, solved the transient oil film pressure via a numerical method, and identified the DCCEs. The results indicate that when the boss height of the inner and outer films are the same, the damping magnitude offered by the inner and outer oil films is nearly the same. In addition, the boss height is the most important factor affecting the DCCEs, followed by the elastic ring thickness and the boss number. Wang et al. [23] established the fluid–structure coupling model of ERSFD by using a numerical method and obtained the oil film pressure, oil film force, and elastic ring deformation of ERSFD. Moreover, based on the Centered Circular Orbit (CCO) assumption, the dynamic characteristic coefficients of ERSFD were further identified. Zhou et al. [24] established a bidirectional fluid–structure coupling model of ERSFD to explore the impact of the elastic ring boss number, geometric size, and inner and outer oil film clearance on the dynamic characteristics of the oil film. Moreover, the study demonstrates that the contribution of the outer oil film to the stiffness is large, while the contribution of the inner oil film to the damping is large. We find that the relatively small inner oil film clearance and large outer oil film clearance are conducive to the enhancement of the oil film damping and the suppression of the nonlinear oil film stiffness. With the decreasing width, height and number of the elastic ring bosses or the growth of the elastic modulus, the stiffness and damping of the inner and outer oil film are accordingly increased. Zhang et al. [25] studied the dynamic characteristic parameters of ERSFD and analyzed the elastic ring deformation with the finite element method. It is verified that the application of the elastic ring can effectively reduce the bearing capacity and the nonlinear degree of oil film stiffness and damping. Moreover, the results suggest that the oil film stiffness is provided by both the inner and outer oil films, while the oil film

damping is mainly provided by the inner oil film. According to the radial deformation of the elastic ring, Qin et al. [26] established a differential calculation model of oil film pressure about ERSFD. The influence of its structural parameters on the characteristics of the oil film force was compared and analyzed. The results show that the elastic ring deformation indirectly changes the thickness of squeeze oil film, while its bosses change the oil film pressure distribution and improve the nonlinearity of the oil film stiffness, which varies with the eccentricity. In addition, the fluid–structure coupling model [23] was constructed by the Mindlin thick plate element in Wang et al. [22] and the three-dimensional solid element in Zhou et al. [24], and the deformation of elastic rings was simulated with the application of the finite element method. This method is demonstrated to be convenient to deal with variable operating conditions and complex assembly performance and can obtain accurate oil film force and then more accurate oil film stiffness and damping. However, it is not conducive to establish a mathematical model and deduce general rules, and there is no comprehensive analysis of the impact of relevant parameters on its dynamic characteristics combined with the complex structure of ERSFD. Novikov and Diligenskii [27] proposed the ERSFD structure of a single-layer ring and double-layer ring for the first time and carried out finite element modeling and verification of single-layer ERSFD structures. However, due to the complexity of ERSFD structures, the mathematical modeling was difficult.

To describe its vibration reduction and frequency modulation mechanism more deeply and accurately, the present study takes the rigid–elastic–oil coupled ERSFD structure as the research object, selects the typical parameters representing the journal, elastic ring and oil film, and establishes the rigid–elastic–oil coupled mathematical model of ERSFD. Because the elastic ring deformation affects the oil film pressure performance when the rotor vibrates at multiple critical speeds, its deformation is obtained following the planar bending theory of a thin-walled ring. Based on the numerical analysis method, the DCCES are solved. In addition, we investigate the effect of journal eccentricity, oil film radius clearance and elastic ring parameters on the DCCEs in this study.

2. Rigid–Elastic–Oil Coupled Mathematical Model of ERSFD

In order to further advance the study of the ERSFD mathematical model, the rigid–elastic–oil coupled mathematical model of ERSFD is analyzed and established from three aspects, including the journal, elastic ring and oil film, respectively. Finally, we can obtain the DCCEs.

2.1. Equation of the Journal Motion

Considering the nonlinear excitation of the system introduced by the unbalanced force of the rotor, the force diagram of the damper journal is shown in Figure 2, in which only the uniform oil film distribution pressure in the inner oil film region between the two adjacent inner bosses is drawn.

Supposing that the journal performs synchronous precession, the differential equation of its motion is established according to Newton’s second law [28].

$$m \frac{d^2 \vec{r}}{dt^2} = \vec{F}_u + \sum \vec{T}_i + \vec{F}_p \quad (1)$$

where \vec{F}_u is the unbalanced force on the journal, $\vec{F}_u = mu_c \Omega^2$, u_c is the imbalanced eccentricity of the journal, Ω refers to the precession angular velocity of the journal, m is the mass of the damper journal (mass sum of bearing assembly and rotor), \vec{T}_i is the boss support force of the elastic ring, $\vec{T}_i = k\delta_i$, i is position number of the inner boss, k stands for the stiffness of the elastic ring, δ_i is the amount of deformation at the elastic ring boss and \vec{F}_p indicates the oil film reactions in the inner cavity.

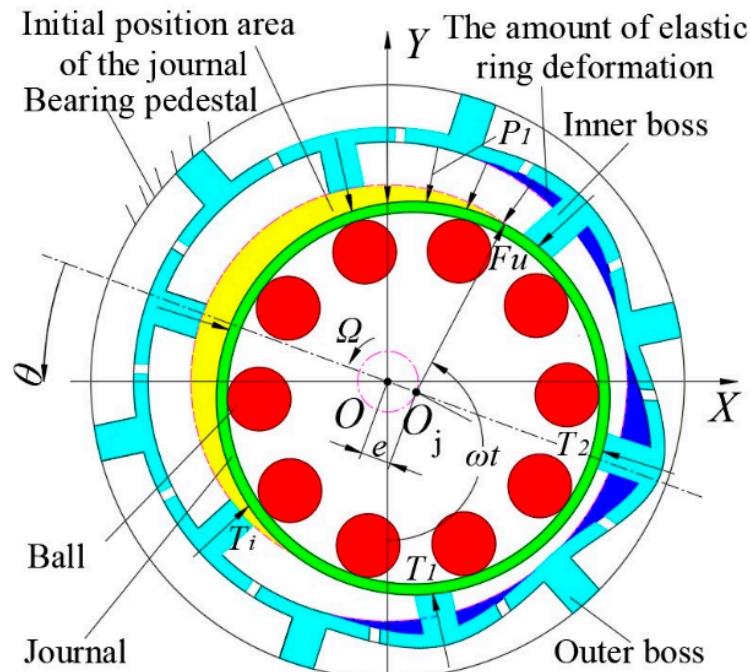


Figure 2. Schematic plot of the force on the journal.

2.2. Governing Equations of the Oil Film Pressure

In terms of the fluid in rigid–elastic–oil coupled model of ERSFD, according to the Navier–Stokes (N-S) equation and the flow continuity equation, the oil film pressure governing equations of ERSFD [29] are expressed as follows:

$$\frac{1}{R^2} \frac{\partial}{\partial \theta} \left[h_i^3 \frac{\partial p}{\partial \theta} \right] + \frac{\partial}{\partial z} \left[h_i^3 \frac{\partial p}{\partial z} \right] = -12\mu\Omega \left[\frac{\partial h_i}{\partial \theta} - \frac{\partial k_e}{\partial \theta} \right] + 12\mu v_d \tag{2}$$

$$\frac{1}{R^2} \frac{\partial}{\partial \theta} \left[h_o^3 \frac{\partial p}{\partial \theta} \right] + \frac{\partial}{\partial z} \left[h_o^3 \frac{\partial p}{\partial z} \right] = -12\mu v_d \tag{3}$$

where θ refers to the circumferential coordinate, z indicates the axial coordinate, μ is the fluid dynamic viscosity, h_i indicates the oil film thickness of the inner cavity, h_o represents the oil film thickness of the outer cavity, R indicates the radius of the journal, k_e represents the elastic ring deformation and v_d suggests the fluid net outflow rate at the damping hole.

2.3. Determination of the Oil Film Thickness (Taking the Elastic Ring Deformation into Account)

As can be seen from Figure 3, the oil film thickness equation in Equations (2) and (3) is as follows:

$$\begin{cases} h_i = C1 + e \cos \theta + h_t + k_e \\ h_o = C2 - k_e \end{cases}, (0 \leq \theta < 2\pi) \tag{4}$$

where $C1$ represents the inner oil film radius clearance, e denotes the eccentricity of the journal, θ refers to angular coordinates which are calculated from the maximum oil film clearance, h_t represents the oil film thickness at the i^{th} boss, $C2$ represents the outer oil film radius clearance and $C1 = C2$.

Because the elastic ring does not rotate relative to the bearing pedestal, the angle between the starting position of the inner boss $\theta_i (i = 1)$ and Y is β , the angle between the adjacent inner boss and the outer boss is π/N , $2\pi/N$ is the angle between the adjacent same side boss and φ is the attitude angle of the journal. When considering the boss height, we can write the oil film thickness at the boss as follows [30]:

$$h_t = \begin{cases} e \cos(\pi + \theta_i - \varphi), \theta_i = \beta + 2\pi(i - 1)/N, i = 1, 2, 3, \dots, N \\ 0, else \end{cases} \tag{5}$$

where θ_i stands for the angle between the i^{th} boss and the offset line.

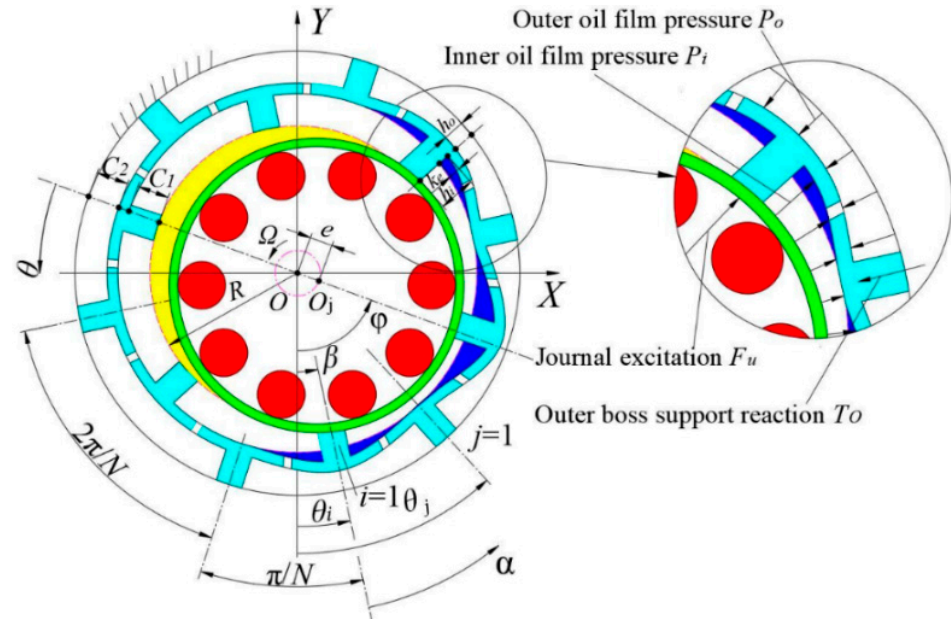


Figure 3. Force deformation diagram of the elastic ring.

The force equation of the elastic ring in Figure 3 is as follows:

$$F_{total} = F_u + T_o + F_{P_i} + F_{P_o} \tag{6}$$

where T_o is outer boss support reaction, F_{P_i} is inner oil film force and F_{P_o} is outer cavity oil film reaction.

Since the force of the elastic ring is generally less than the load exerted directly on the elastic ring by the damper journal, the influence of the oil film force on the elastic ring deformation is ignored. In addition, the deformation of the elastic ring is mainly columnar bending, regardless of the axial deformation of the elastic ring. Because the ratio between the thickness of the elastic ring and its mean radius of curvature is less than 0.05, the elastic ring is featured with a thin-walled ring. In addition, the differential equation of radial deflection change about the elastic ring at an arbitrary angle ψ is expressed in accordance with the planar bending theory of the thin-walled ring [31].

$$\frac{d^2k_e}{d\psi^2} + k_e = -\frac{Mr_t^2}{EI} \tag{7}$$

where EI is the elastic ring flexural stiffness in the original curvature plane, M indicates the bending moment on the cross section at ψ , M is positive when the outer fiber is compressed or the original curvature is reduced and r_t is the middle diameter of the elastic ring.

Since the elastic ring mainly carries radial load, by using the virtual work principle, the radial deflection corresponding to the ψ at an arbitrary angular position can be obtained [32] and expressed in series form as follows:

$$k_e(\phi_m) = \frac{r_t^3}{4\pi EI} \sum_{i=1}^N q_i (-\phi_m \sin \phi_m + (\phi_m/2 - \pi)\phi_m \cos \phi_m - 2) \tag{8}$$

where ϕ_m is the difference between the position ψ_m of the i^{th} boss force and the position angle ψ of the radial deflection on the elastic ring, N is the boss number of the elastic ring,

q_i is the force exerted on the inner boss, and $q_i = k\delta_i = ke \cos(\theta_i - \varphi)$. Because ϕ_m must be positive and $0 \leq \phi_m \leq 2\pi$, as shown in Figure 4, ϕ_m is represented as follows:

$$\begin{cases} \phi_m = \psi_m - \psi, \psi_m > \psi \\ \phi_m = 2\pi - \psi + \psi_m, \psi_m < \psi \end{cases} \quad (9)$$

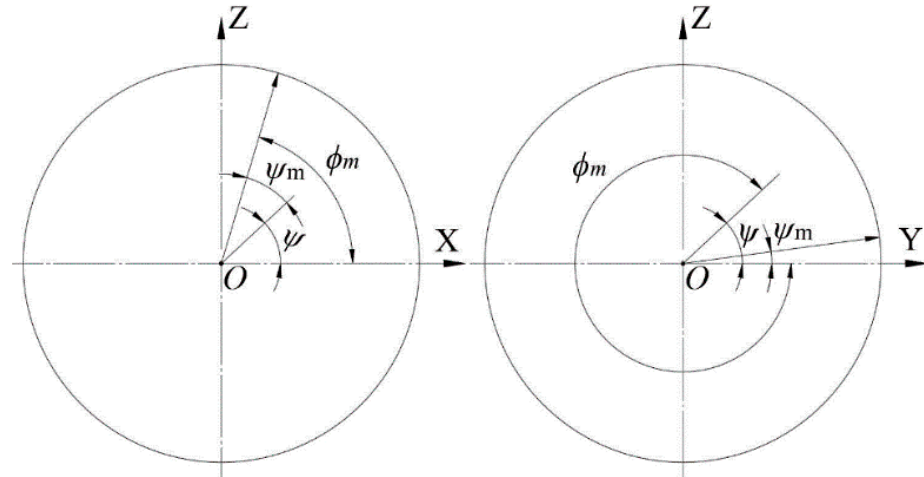


Figure 4. Diagram of deformation angle of the elastic ring.

2.4. Oil Film Pressure Solution

Based on the rigid–elastic–oil coupled ERSFD, the total number of nodes divided alongside the circumferential and axial directions of the solution region are equal to m and n , respectively, and the corresponding step sizes are $2\pi/m$ and $2/n$, as revealed in Figure 5.

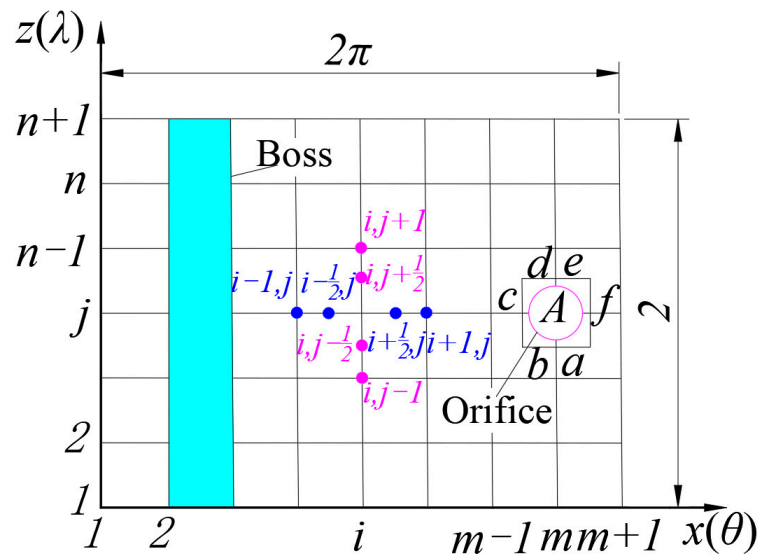


Figure 5. Diagram of the oil film discrete region.

The solution domain of the oil film is found to be discontinuous due to the presence of the boss and the damping hole. Taking the oil film of the inner cavity as an example, for the micro element column with oil film thickness of $h(h = h_i)$, the volume flow alongside the circumferential and axial directions are as follows:

$$\begin{cases} Q_x = -h_i^3/12\mu \frac{\partial p}{\partial x} - R\Omega h_i \\ Q_z = -h_i^3/12\mu \frac{\partial p}{\partial z} \end{cases} \quad (10)$$

where Q_x is the circumferential volume flow and Q_z is the axial volume flow.

According to the conservation of control volume flow, the flow rate Q_A of the damping hole is expressed by the Hagen–Poiseuille formula [33]:

$$Q_A = \frac{d_0^2}{32\mu} \frac{A}{h_s} \Delta p \tag{11}$$

where Q_A is the volume flow from the inner oil chamber to the outer oil chamber, d_0 refers to the diameter of the damping hole, h_s is the depth of the damping hole (also known as the elastic ring thickness), A indicates the cross-sectional area of the damping hole and Δp refers to differential pressure along the depth of the hole.

v_d in Equations (2) and (3) can be calculated by the following formula:

$$v_d = d_0^2 R^2 \Delta p \Omega / (16C1^2 h_s) \tag{12}$$

ERSFD is equipped with sealing rings at both ends to prevent oil leakage. When the elastic ring is stably stressed and no longer deforms, the change in oil film pressure along the axial direction is approximately zero. Then, in the whole oil film discrete region, the pressure boundary conditions [34–36] are as follows:

$$\begin{cases} \frac{\partial p}{\partial n} \Big|_{z=0} = \frac{\partial p}{\partial n} \Big|_{z=L} = 0 \\ p(\theta = 0, z) = p(\theta = 2\pi, z) = p_s \end{cases} \tag{13}$$

Define the dimensionless parameter as $X = R\theta(0 \leq \theta \leq 2\pi)$, $\lambda = 2z/L(-1 \leq \lambda \leq 1)$, $H = h_i/C1$, $P = p/p_s$, $\varepsilon = e/C1$ and $p_s = 2\Omega\mu R^2/C1^2$. Combined with Equations (2), (3), (11) and (12), the five-point central finite difference method can be used to obtain the following:

$$W_{i,j}P_{i-1,j} + C_{i,j}P_{i,j} + E_{i,j}P_{i+1,j} + N_{i,j}P_{i,j+1} + S_{i,j}P_{i,j-1} = F_{i,j} \tag{14}$$

where $W_{i,j} = H_{i-1/2,j}^3$, $C_{i,j} = W_{i,j} + E_{i,j} + N_{i,j} + S_{i,j}$, $E_{i,j} = H_{i+1/2,j}^3$, $N_{i,j} = [2R\Delta\theta/(L\Delta\lambda)]^2 H_{i,j+1/2}^3$ and $S_{i,j} = [2R\Delta\theta/(L\Delta\lambda)]^2 H_{i,j-1/2}^3$. For the inner cavity, $F_{i,j} = 6\varepsilon \sin \theta - 3d_0^2 R^2 \Delta p / (8h_s C1^3)$. For the outer cavity, $F_{i,j} = 3d_0^2 R^2 \Delta p / (8h_s C1^3)$.

Equation (14) is constructed into an overrelaxation iteration scheme:

$$P_{i,j} = \frac{\sigma}{C_{i,j}} (F_{i,j} - E_{i,j}P_{i+1,j} - W_{i,j}P_{i-1,j} - NP_{i,j+1} - SP_{i,j-1}) + (1 - \sigma)P_{i,j} \tag{15}$$

where σ is the relaxation factor and $\sigma = 1.5$.

Assuming that the iteration accuracy follows the relative error convergence criterion, then, we can obtain the following:

$$\frac{\sum_{i=1}^{m+1} \sum_{j=1}^{n+1} |P_{i,j}^{(kk)} - P_{i,j}^{(kk-1)}|}{\sum_{i=1}^{m+1} \sum_{j=1}^{n+1} |P_{i,j}^{(kk)}|} \leq \delta \tag{16}$$

where kk is iterative times and δ is iteration accuracy.

2.5. DCCEs Solution

The DCCEs depend on the radial and axial components of ERSFD oil film pressure acting on the journal. By applying Simpson’s rule, we can solve the integration alongside the axial direction [37]:

$$S(i) = p_s \int_{-\frac{l}{2}}^{\frac{l}{2}} P(\theta, \lambda) d\lambda \approx \frac{p_s L}{6n} \left(\begin{matrix} (P_{i,1} + P_{i,n+1}) \\ +2(P_{i,3} + P_{i,5} + \dots + P_{i,n-1}) \\ +4(P_{i,2} + P_{i,4} + \dots + P_{i,n}) \end{matrix} \right) \tag{17}$$

By the same token, the integral along the circumference is as follows:

$$W_x \approx -\frac{2\pi}{6m} R \left(\begin{array}{l} (S_1 \cos(\theta_1 - \varphi) + S_{m+1} \cos(\theta_{m+1} - \varphi)) \\ +2(S_3 \cos(\theta_3 - \varphi) + S_5 \cos(\theta_5 - \varphi) + \dots + S_{m-1} \cos(\theta_{m-1} - \varphi)) \\ +4(S_2 \cos(\theta_2 - \varphi) + S_4 \cos(\theta_4 - \varphi) + \dots + S_m \cos(\theta_m - \varphi)) \end{array} \right) \quad (18)$$

$$W_y \approx -\frac{2\pi}{6m} R \left(\begin{array}{l} (S_1 \sin(\theta_1 - \varphi) + S_{m+1} \sin(\theta_{m+1} - \varphi)) \\ +2(S_3 \sin(\theta_3 - \varphi) + S_5 \cos(\theta_5 - \varphi) + \dots + S_{m-1} \sin(\theta_{m-1} - \varphi)) \\ +4(S_2 \sin(\theta_2 - \varphi) + S_4 \sin(\theta_4 - \varphi) + \dots + S_m \cos(\theta_m - \varphi)) \end{array} \right) \quad (19)$$

where W_x refers to the radial force of the oil film, and W_y denotes the tangential force of the oil film.

According to Equations (17)~(19), the formula for solving the DCCEs is as follows:

$$\begin{cases} Ke = -\frac{W_x}{e} \\ Ce = -\frac{W_y}{e\Omega} \end{cases} \quad (20)$$

In summary, the flow chart for solving the DCCEs can be found in Figure 6.

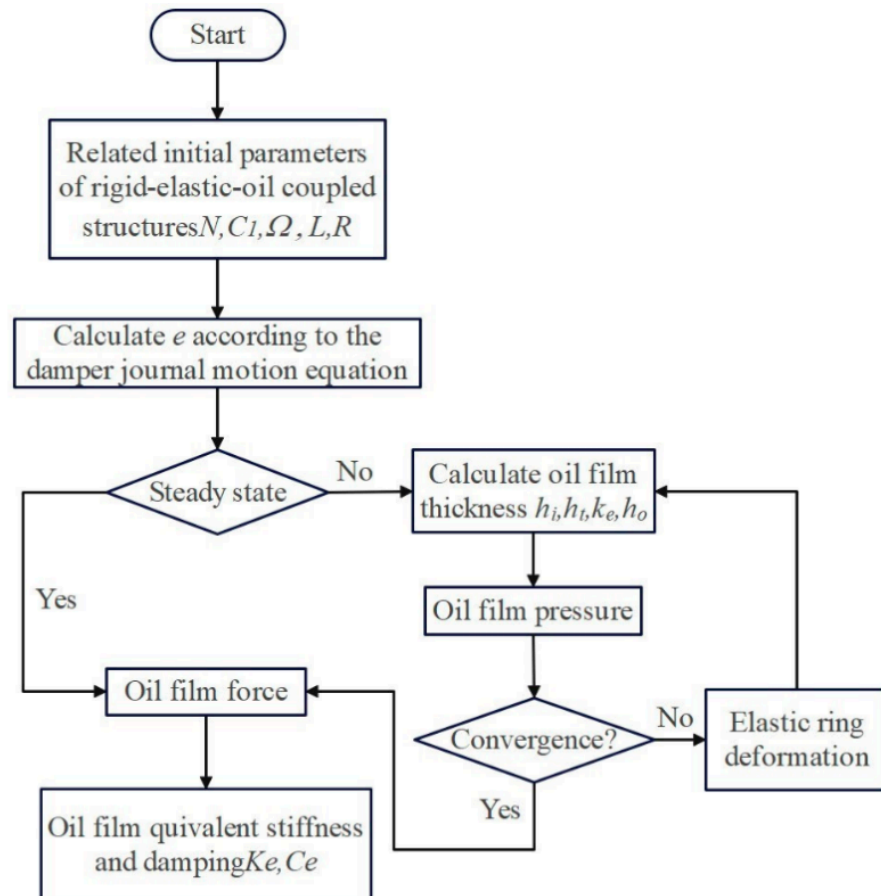


Figure 6. Flow chart for solving the DCCEs.

3. Results, Analysis and Discussion

3.1. Influence of the Eccentricity on the DCCEs

The eccentricity $\varepsilon = e/c$ ($c = C1$ or $C2$) of the journal is set as 0.3, 0.4, 0.5, 0.6 and 0.7, respectively. In addition, we achieve the DCCEs, as displayed in Figure 7.

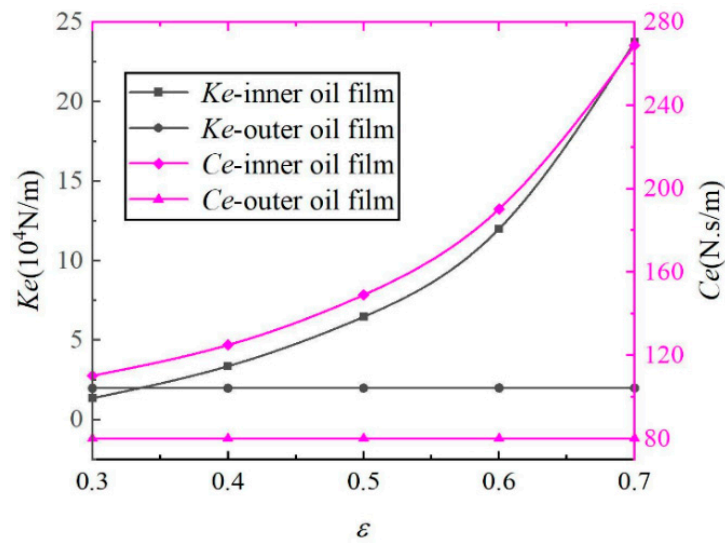


Figure 7. Influence of the eccentricity on equivalent stiffness Ke and damping Ce .

On the basis of Figure 7, it can be seen that when the journal eccentricity shows the tendency of increase, the oil film pressure of ERSFD accordingly elevates. At the same time, the increase can also be found in the oil film equivalent stiffness Ke and damping Ce . Apart from that, the equivalent stiffness Ke and damping Ce of the oil film in the inner cavity are found to be greater than those in the outer cavity, which is demonstrated to be a result of the oil film shear as well as the squeeze in the inner cavity. However, it is observed that the nonlinear degree of the oil film equivalent stiffness Ke and damping Ce in the inner cavity is higher than that in the outer cavity.

3.2. Influence of the Oil Film Radius Clearance on the DCCEs

In this study, the eccentricity is set as 0.5, with the precession angular velocity of the journal being 942 rad/s. We can take the oil film radius clearance of the inner cavity to be 0.3, 0.4, 0.5, 0.6 and 0.7 mm in turn. Then, the computation of the dynamic coefficient of the oil film can thus be performed. In accordance with Figure 8, the findings obtained are revealed in the present study.

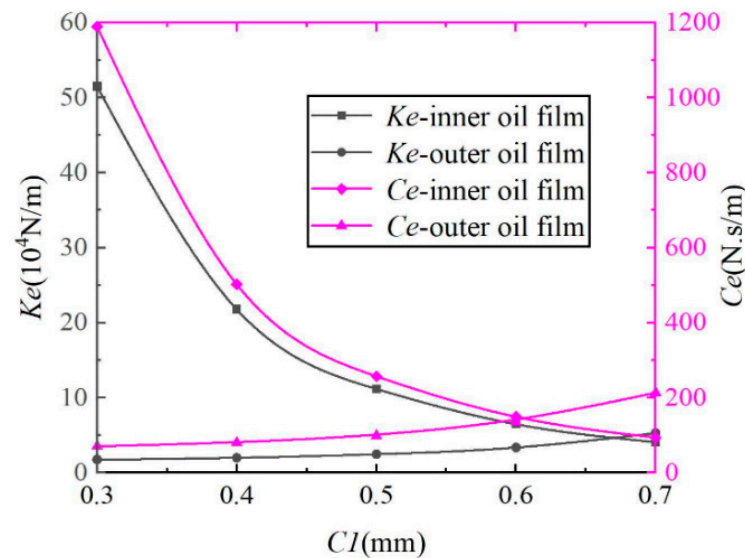


Figure 8. Impact of the oil film radius clearance on equivalent stiffness Ke and damping Ce .

In accordance with Figure 8, the oil film equivalent stiffness Ke and damping Ce in the inner cavity decrease with the increasing oil film radius clearance on the premise that

the sum of oil film clearance in the inner and outer cavities remains unchanged and the eccentricity of the journal is a constant value. However, when the oil film radius clearance decreases, there also exists growth in the oil film equivalent stiffness Ke and damping Ce in the outer cavity. Moreover, it is shown that the abovementioned findings are consistent with the literature [24]. Additionally, relative to that in the outer cavity, we can find that the nonlinear degree of the oil film equivalent stiffness Ke and damping Ce in the inner cavity is also shown to be higher.

3.3. Influence of the Flexibility Coefficient on the DCCEs

The values considered for the flexibility coefficient of the elastic ring ($\alpha = r_t^3/4\pi EI$) are 9.0×10^{-5} m/N, 7.0×10^{-4} m/N, 5.0×10^{-3} m/N, 3.0×10^{-2} m/N and 1.0×10^{-1} m/N. DCCEs are calculated and Figure 9 displays the findings.

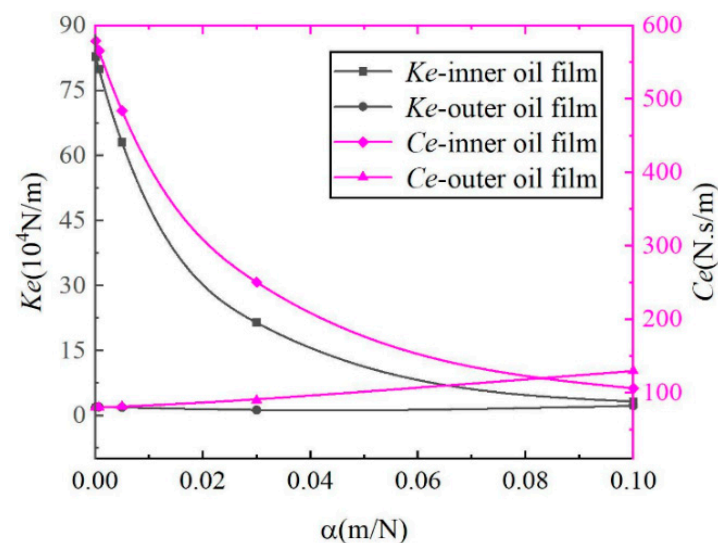


Figure 9. Effect of the flexibility coefficient on equivalent stiffness Ke and damping Ce .

As described in Figure 9, with the increasing flexibility coefficient, we can also find obvious elevation in the deformation of the elastic ring. Simultaneously, the thickness of inner cavity oil film increases and the thickness of outer cavity oil film decreases. As a result, the equivalent stiffness Ke and damping Ce of the inner cavity oil film gradually decrease, while the equivalent stiffness Ke and damping Ce of the outer cavity oil film gradually increase. Additionally, the changes in oil film equivalent stiffness Ke and damping Ce amplitude in the inner cavity are smaller and the nonlinear degree is higher than that in the outer cavity.

3.4. Influence of the Damping Hole Diameter on the DCCEs

The damping hole diameter of the elastic ring is successively taken as 0.6 mm, 0.8 mm, 1.0 mm, 1.2 mm and 1.5 mm. DCCEs can be accessed and Figure 10 shows the findings.

Form the Figure 10, we can see that the oil film equivalent stiffness Ke within the inner and outer cavities gradually lowers but the oil film equivalent damping Ce gradually increases with the increase in the damping hole diameter in the elastic ring. This is because the larger the diameter of the damping hole, the more oil flow through the damping hole per unit time, which indirectly weakens the squeeze effect of the oil film, resulting in the reduction in the oil film pressure and thus the oil film equivalent stiffness Ke . At the same time, the more oil through the oil hole, the more energy taken away and the greater the damping. Furthermore, the data indicate that the oil film equivalent stiffness Ke and damping Ce of the inner and outer cavities have small changes.

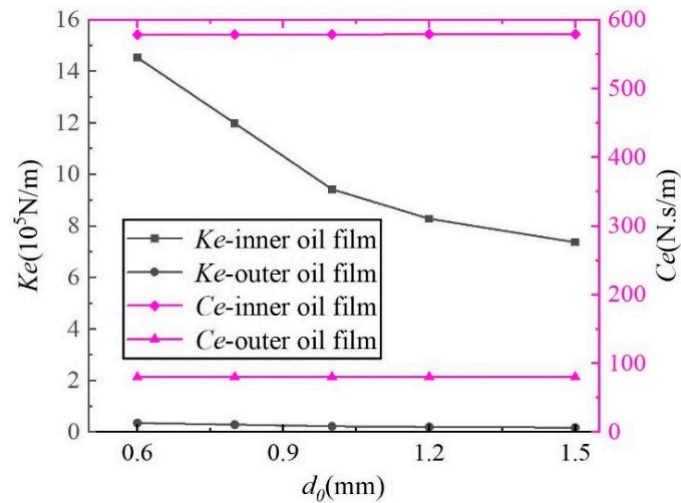


Figure 10. Effect of the damping hole diameter on equivalent stiffness Ke and damping Ce .

4. Sensitivity Analysis

4.1. The Optimal Impact Factor Determination

Different parameters have different effects on the DCCEs. It is necessary to determine the dynamic oil film reaction associated with the bearing outer ring precession in solving the dynamic differential equations of aeroengine main ball bearing based on rigid–elastic–oil coupling. Therefore, according to Figure 11, we can contrast and explore the impact of each parameter on the DCCEs qualitatively by taking the oil film equivalent stiffness Ke and damping Ce of the inner cavity as an example.

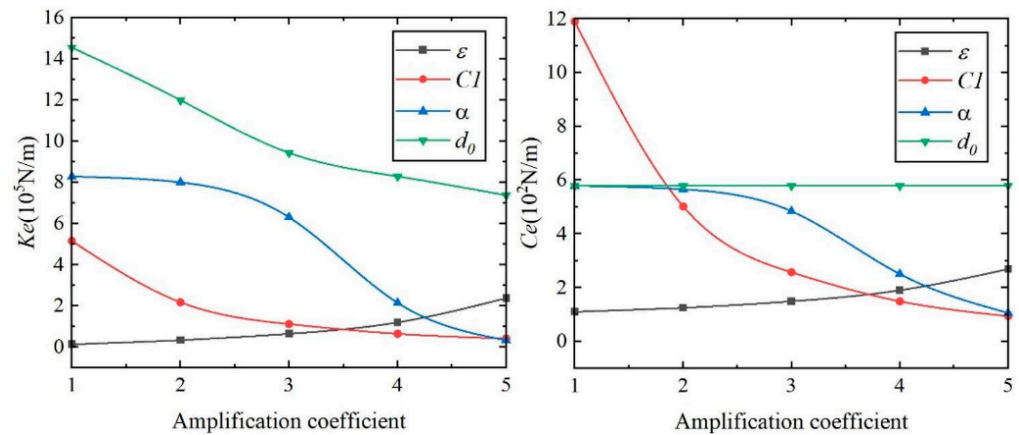


Figure 11. Influence of relevant parameters on the DCCEs.

Within the value range of all relevant parameters, combined with the results obtained from 3.1 to 3.4, the confidence interval is selected as 95%, and the linear regression method is adopted to calculate the sensitivity coefficient of each parameter. Table 1 presents the calculation results.

Table 1. Sensitivity coefficients of each parameter.

| Parameter | Sensitivity Coefficient | |
|--|-------------------------|-------|
| | Ke | Ce |
| Journal eccentricity ϵ | 0.534 | 0.383 |
| Oil film radius clearance $C1$ (mm) | 1.101 | 2.545 |
| Flexibility coefficient α (m/N) | 7.537 | 4.548 |
| Diameter of damping hole d_0 (mm) | 0.800 | 0.089 |

As shown in Table 1, the elastic ring flexibility coefficient has the greatest effect on the DCCEs. Therefore, the elastic ring flexibility coefficient could be taken as the most important factor in the optimization design of ERSFD structures.

4.2. Influence of the Optimum Influence Factor on Inner Oil Film Pressure

As can be seen from Figure 12, the values considered for flexibility coefficient of the elastic ring are $7.0 \times 10^{-4} \text{ m/N}$, $3.0 \times 10^{-2} \text{ m/N}$ and $1.0 \times 10^{-1} \text{ m/N}$, then the dimensionless maximum pressure of the oil film in the inner cavity decreases from 2.3424 to 0.01191. The results indicate that the greater the flexibility coefficient is, the easier the elastic ring is to deform, and the thickness of the oil film in the inner cavity increases. The squeeze and shear effects of the oil film are weakened, and the pressure of the oil film gradually decreases, which ultimately leads to the decrease in the oil film reaction force on the journal. The above results are in good agreement with the simulation results in reference [30].

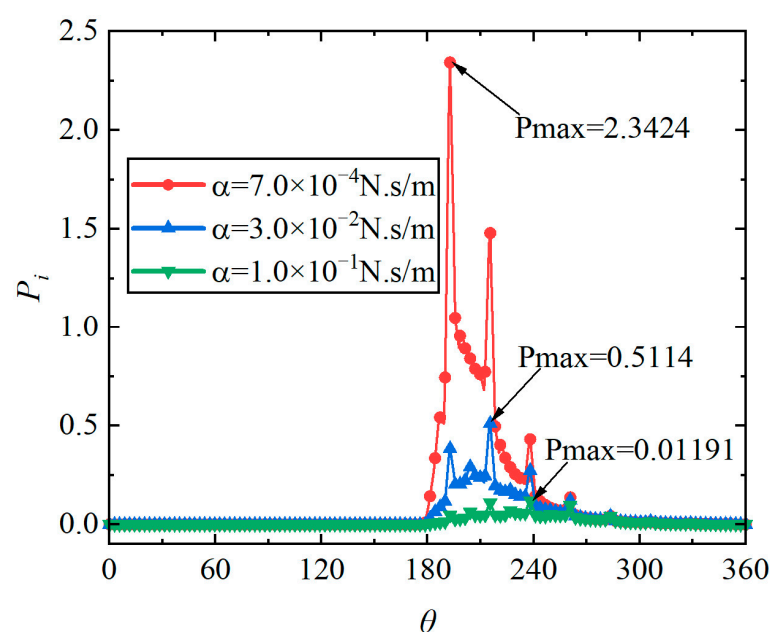


Figure 12. Variation of inner oil film pressure with flexibility coefficient.

5. Conclusions

To conclude, the rigid–elastic–oil coupled numerical analysis model of ERSFD was established, the center finite difference method was adopted for solving the oil film pressure and the Simpson method was employed with the aim of solving the DCCEs. The impact of the journal eccentricity, the oil film radius clearance, the flexibility coefficient and the diameter of the damping hole on the DCCEs were studied in this study. The conclusions are as follows:

(1) With the increasing eccentricity of the journal, we can see that the corresponding oil film equivalent stiffness K_e and damping C_e in the inner and outer cavity of the ERSFD elevate, while the degree of nonlinearity in the inner cavity is higher than that in the outer cavity. In addition, the oil film equivalent stiffness K_e of the inner and outer cavities decreases with the increase in the diameter of the damping hole, and the oil film equivalent damping C_e increases with the increase in the diameter of the damping hole, but the change in range of the oil film equivalent stiffness K_e and damping C_e of the inner and outer cavities is small.

(2) On the premise that the total oil film clearance and the eccentricity of the journal are constant, the elevation of the oil film clearance and flexibility of the elastic ring within the inner cavity results in the decreasing oil film equivalent stiffness K_e and damping C_e in the inner cavity, as well as the increasing oil film equivalent stiffness K_e and damping C_e in

the outer cavity. In addition, relative to that in the outer cavity, the nonlinear degree of the oil film in the inner cavity is shown to be higher.

(3) According to linear regression analysis, it can be concluded that the influence degrees of the elastic ring flexibility coefficient on the oil film equivalent stiffness K_e and damping C_e is largest, followed by the oil film radius clearance. The eccentricity of the journal and the damping hole diameter are relatively small. When the flexibility coefficient increases from 7.0×10^{-4} m/N to 1.0×10^{-1} m/N, the oil film pressure in the cavity decreases from 2.3424 to 0.01191.

Author Contributions: Conceptualization, Y.L.; visualization, Y.L.; data curation, Y.L.; formal analysis, Y.L.; methodology, Y.L.; validation, Y.L. and H.Y.; writing—original draft preparation, Y.L.; writing—review and editing, Y.L., H.Y. and S.D.; resources, S.D.; supervision, Y.L., H.Y. and S.D. All authors have read and agreed to the published version of the manuscript.

Funding: This study was supported by the National Natural Science Foundation of China (Grant No. 51905152).

Data Availability Statement: The datasets supporting the conclusions of this article are included within the article.

Conflicts of Interest: The authors declare no conflict of interest.

References

- Wang, Z.; Xu, N.; Yu, X.; Liu, Z.; Zhang, G. The dynamic characteristic analysis of elastic ring squeeze film damper by fluid-structure interaction approach. In Proceedings of the ASME Turbo Expo 2017: Turbomachinery Technical Conference and Exposition, Charlotte, NC, USA, 26–30 June 2017; pp. 26–30.
- Ibrahim, R.A. Recent advances in nonlinear passive vibration isolators. *J. Sound Vib.* **2008**, *314*, 371–452. [[CrossRef](#)]
- Balyakin, V.B. Advanced designs of elastic damper supports for aircraft engine rotors. *Russ. Aeronaut.* **2015**, *58*, 42–47. [[CrossRef](#)]
- Cao, L.; Jiang, H.F. Preliminary study on vibration reduction mechanism of elastic ring squeeze film damper. *J. Vib. Eng.* **2007**, *20*, 584–588.
- Zhao, L.; Liao, M.F.; Wang, S.J.; Liu, Q.Y.; Hou, L.Z. Experimental study on vibration reducing effect of elastic ring squeeze film damper. *J. Propuls. Technol.* **2021**, *42*, 1129–1137.
- Han, B.; Ding, Q. Forced responses analysis of a rotor system with squeeze film damper during flight maneuvers using finite element method. *Mech. Mach. Theory* **2018**, *122*, 233–251. [[CrossRef](#)]
- Younan, A.A.; Cao, J.; Dimond, T.W.; Allaire, P.E. Nonlinear analysis of squeeze film damper with entrained air in rotor dynamic systems. *Tribol. Trans.* **2010**, *54*, 132–144. [[CrossRef](#)]
- Gjika, K.; San Andres, L.; LaRue, G.D. Nonlinear dynamic behavior of turbocharger rotor bearing systems with hydrodynamic oil film and squeeze film damper in series: Prediction and experiment. *J. Comput. Nonlinear Dyn.* **2010**, *5*, 2040–2049. [[CrossRef](#)]
- Liu, Z.C.; Liao, M.F.; Cong, P.H.; Wang, J.; Wang, S.J.; Shi, B.; Li, Y. Design method of squeeze film damper for aero-engine rotors. *J. Aerosp. Power.* **2015**, *30*, 2762–2770.
- Jiang, H.; Shen, Y.; Yi, M. Power of the fourth generation fighter aircraft-visiting professor Chen guang-the famous aeroengine expert in our country. *Ordnance Ind. Sci. Technol.* **2009**, *6*, 6.
- Lin, Z.M. The current development and future trends of fighter engines. *Aeroengine* **2006**, *32*, 1–8.
- Wu, S.T. Research on military aircraft technology status and prospect of future development trend. *Mech. Electr. Inf.* **2019**, *21*, 146–147.
- Zhou, M. Study on vibration damping mechanism of an elastic ring squeeze film damper. *J. Aerosp. Power.* **1998**, *13*, 403–407.
- Hong, J.; Deng, Y.; Zhang, D.Y. Dynamic design method of elastic ring squeeze oil film Damper. *J. Beijing Univ. Aeronaut. Astronaut.* **2006**, *32*, 649–653.
- Xu, Y.; Chen, X.; Zou, J.; Qi, W. Influence of Orifice Distribution on the Characteristics of Elastic Ring-Squeeze Film Dampers for Flywheel Energy-Storage System. *IEEE Trans. Plasma Sci.* **2013**, *41*, 1272–1279. [[CrossRef](#)]
- Li, B.; Cheng, D.C.; Jiang, Z.M. Experiment study on dynamic characteristics of elastic ring squeeze film damper rotor system. *Gas Turbine Exp. Res.* **2015**, *28*, 19–22.
- Han, Z.F.; Ding, Q.; Zhang, W. Dynamical analysis of an elastic ring squeeze film damper-rotor system. *Mech. Mach. Theory* **2019**, *131*, 406–419. [[CrossRef](#)]
- Shi, M.; Yang, Y.; Deng, W.; Wang, J.; Fu, C. Analysis of dynamic characteristics of small-scale and low-stiffness ring squeeze film damper-rotor system. *Appl. Sci.* **2022**, *12*, 7167. [[CrossRef](#)]
- Zhao, L.; Liao, M.; Niu, J. Investigation on steady state unbalance response of rotor with elastic ring squeeze film damper. *IOP Conf. Ser. Mater. Sci. Eng.* **2020**, *751*, 012043. [[CrossRef](#)]
- Cao, L.; Gao, D.P.; Jiang, H.F. Investigation on design factor of elastic ring squeeze film damper. *Gas Turbine Exp. Res.* **2006**, *19*, 30–34.

21. He, H.; Wang, S.H.; Wang, L.Q.; Ji, J.B.; Zhao, L.L. Effect of elastic ring damper on dynamic performance of turbocharger rotor. *Veh. Engine* **2016**, *4*, 70–74+81.
22. Wang, Z.L.; Liu, Z.S.; Zhang, G.H. Numerical modelling of elastic ring squeeze film damper based on thick plate and force coefficient identification. *J. Aerosp. Power* **2019**, *34*, 635–642.
23. Wang, Z.L.; Liu, Z.S.; Xu, N. Modeling and dynamic characteristics investigation of elastic ring squeeze film damper by fluid-structure interaction approach. *Turbine Technol.* **2020**, *62*, 5.
24. Zhou, H.; Zhang, C.; Ai, Y.; Sun, D.; Chen, X. Study on Dynamic Characteristics and modeling of elastic ring squeeze film damper based on fluid-structure interaction. *J. Mech. Eng.* **2020**, *56*, 195–205.
25. Zhang, W.; Ding, Q. Elastic ring deformation and pedestal contact status analysis of elastic ring squeeze film damper. *J. Sound Vib.* **2015**, *346*, 314–327. [[CrossRef](#)]
26. Qin, Y.J.; Liu, B.B.; Yin, B.F.; Hao, L.; Zhao, Q.J.; Zhao, W. Influence of elastic ring structural parameters on ERSFD dynamic system characteristics. *J. Aerosp. Power.* **2023**, 1–10. [[CrossRef](#)]
27. Novikov, D.K.; Diligenskii, D.S. The development of a squeeze film damper parametric model in the context of a fluid-structural interaction task. *IOP Conf. Ser. Mater. Sci. Eng.* **2018**, *302*, 012008. [[CrossRef](#)]
28. Zhou, M.; Li, Q.H.; Yan, L.T. Research on vibration reduction mechanism of elastic ring squeeze film damper (1)-model of vibration reduction mechanism of elastic ring squeeze film damper. *Gas Turbine Exp. Res.* **1998**, *11*, 19–33.
29. Zhou, M.; Li, Q.H.; Yan, L.T. Research on damping mechanism of elastic ring squeeze Film Damper (2)-solution of oil film force characteristics of elastic ring squeeze film damper. *Gas Turbine Exp. Res.* **1999**, *12*, 30–33.
30. Yang, X.M.; Yang, H.S.; Cui, Y.C.; Li, Y.; Jiang, B.; Deng, S. Pressure performance for a thin-walled ring and turbulent-jet orifice modeled elastic squeeze film damper. *Chin. J. Aeronaut.* **2022**, *35*, 235–251. [[CrossRef](#)]
31. Kurajian, G.M.; Na, T.Y. Thin elastic rings subjected to radial load sets. *J. Eng. Ind.* **1972**, *71*, 783–788. [[CrossRef](#)]
32. Liu, J.Y.; Chiu, Y.P. Analysis of a Thin Elastic Ring under Arbitrary Loading. *J. Eng. Ind.* **1974**, *96*, 870. [[CrossRef](#)]
33. Deng, Y.; Lin, L.; Shi, Y.J. Dynamic design method of elastic ring squeeze film damper. *J. Beijing Univ. Aeronaut. Astronaut.* **2006**, *32*, 531–535.
34. Tichy, J.A. A Study of the Effect of Fluid Inertia and End Leakage in the Finite Squeeze Film Damper. *J. Tribol.* **1987**, *109*, 54. [[CrossRef](#)]
35. Леонтьев, М.; Degtiarev, S.A. Mathematical models of squeeze film damper in gas turbine engine rotor support. *Aerosp. Mech. Eng.* **2017**, *16*, 115–128.
36. Kutakov, M.N.; Degtiarev, S.A.; Leontiev, M.K. Mathematical models of squeeze film dampers in rotor dynamics of gas turbine engines. *VESTNIK Samara Univ. Aerosp. Mech. Eng.* **2017**, *16*, 115. [[CrossRef](#)]
37. Chen, W.; Chen, S.; Hu, Z.; Tang, J.; Li, H. A novel dynamic model for the spiral bevel gear drive with elastic ring squeeze film dampers. *Nonlinear Dyn.* **2019**, *98*, 1081–1105. [[CrossRef](#)]

Disclaimer/Publisher’s Note: The statements, opinions and data contained in all publications are solely those of the individual author(s) and contributor(s) and not of MDPI and/or the editor(s). MDPI and/or the editor(s) disclaim responsibility for any injury to people or property resulting from any ideas, methods, instructions or products referred to in the content.